

On the applicability of Kerker preconditioning scheme to the self-consistent density functional theory calculations of inhomogeneous systems

Yuzhi Zhou,^{1,2} Han Wang,^{1,2} Yu Liu,^{1,2} Xingyu Gao,^{1,2} and Haifeng Song^{1,2}

¹*Institute of Applied Physics and Computational Mathematics,
Beijing 100094, People's Republic of China*

²*CAEP Software Center for High Performance Numerical Simulation,
Beijing 100088, People's Republic of China*

(Dated: December 14, 2024)

Abstract

Kerker preconditioner, based on the dielectric function of homogeneous electron gas, is designed to accelerate the self-consistent field (SCF) iteration in the density functional theory (DFT) calculations. However, question still remains regarding its applicability to the inhomogeneous systems. In this paper, we develop a modified Kerker preconditioning scheme which captures the long-range screening behavior of inhomogeneous systems thus improve the SCF convergence. The effectiveness and efficiency is shown by the tests on long- z slabs of metals, insulators and metal-insulator contacts. Without *a priori* knowledge of the system, we design the *a posteriori* indicator to monitor if the preconditioner has suppressed charge sloshing during the iterations. In the circumstances, two schemes of the self-adaptive configuration are developed.

I. INTRODUCTION

Over the past few decades, the Kohn-Sham density functional theory (DFT) calculation [1, 2] has evolved into one of the most popular *ab initio* approaches for predicting the electronic structures and related properties of matters. The computational kernel of the Kohn-Sham DFT calculation is to solve a tangible nonlinear eigenvalue problem, replacing the original difficult many-body problem [2]. The Kohn-Sham equation is usually solved by the self-consistent field (SCF) iteration, which is proved quite reliable and efficient in most cases [3]. However, the well known "charge sloshing" problem is likely to occur in the SCF iterations as the dimension of the system gets large. The charge sloshing generally refers to the long-wavelength oscillations of the output charge density due to some small changes in the input density during the iterations, and results in a slow convergence or even divergence [3–5]. In some cases it might be referred to the oscillation between different local states of the d or f electrons [6]. In this work, we concentrate on the former situation.

Given a fixed number of total atoms, the charge sloshing and poor SCF convergence are more prominent and exacerbated in the long-*z* slab systems, where one dimension of the unit cell is much longer than the other two's. On the other hand, investigating the properties of the surface and interface using DFT calculations has become one important subject in many scientific and technological fields, such as solid state physics, semiconductor processing, corrosion, and heterogeneous catalysis [7, 8]. The surface/interface is generally simulated by the slab model with the periodic boundary condition. When one comes to distinguish the properties between the bulk and the surface, a rather thick slab is needed to fully restore region with bulk-like properties. One example is the calculation of the band offsets and valence band alignment at the semiconductor heterojunctions [9]. To get a quantitatively accurate band offset, the lattice of both semiconductors must be extended far away from the contact region. Similar example is the calculation of work function. Generally speaking, the thick slab calculation requires relative high accuracy and is very likely to encounter charge sloshing. Effective and efficient mixing schemes are therefore needed to speed up the convergence in the surafce/interface calculations.

A practical mixing scheme in the modern DFT code generally takes into account two aspects: one is combining the results from previous iterations to build the input for next step; the other is reflecting the dielectric response of the system (better known as "precond-

intioning”). On the first aspect, Pulay and Broyden-like schemes are well established and widely used [10, 11]. On the second aspect, Kerker in 1981 proposed that charge mixing could be preconditioned by a diagonal matrix in the reciprocal space. This matrix takes the form of inverse dielectric matrix derived from Thomas-Fermi model of homogeneous electron gas [12]. As pointed out in some literature [3, 13, 14], the preconditioning matrix should be an approximation to the dielectric function of the system. In this sense, the Kerker preconditioner is ideal for simple metals such as Na and Al which can be regarded as the homogeneous electron gas. Moreover, for most metallic systems, the Kerker preconditioner is a suitable preconditioner since it describes the dielectric responses at the long wavelength limit fairly well.

A natural question is then raised: can Kerker preconditioner be applied to the non-metallic systems and hybrid systems of metal-insulator contact? Efforts have been made to develop effective preconditioning schemes to accommodate the inhomogeneity. Kresse *et al.* suggest adding a lower bound to the Kerker preconditioner for calculating the large insulating systems [3]. Similarly, Gonze *et al.* realize it with a smoother preconditioning function [15]. Raczkowski *et al.* solve the Thomas Fermi von Weizsäcker equation to directly compute the optimized mixing density, in which process the full dielectric function is implicitly solved [13]. Shiihara *et al.* recast the Kerker preconditioning scheme in the real space [16]. Lin and Yang further proposed an elliptic preconditioner in the real space to better accommodates the SCF calculations of large inhomogeneous systems [17]. Ho *et al.* [18], Sawamura *et al.* [19] and Anglade *et al.* [20] adopt similar preconditioning schemes in which the exact dielectric matrix is computed by the calculated Kohn-Sham orbitals.

An important part of the above works relies on solving the realistic dielectric response either explicitly or implicitly. However, the extra computational overhead cannot be negligible for large-scale systems. In practice, the computational expense to achieve the SCF convergence is more of the concern and a good preconditioner does not necessarily mean solving the dielectric function as accurately as possible. In this paper, we focus on extending the applicability of the Kerker preconditioning model, which is based on the simple form of the Thomas-Fermi screening model. This is achieved by modifying the Kerker preconditioner to better capture the long-range screening behavior of the inhomogeneous systems. For perfect insulating system, we introduce a threshold parameter to represent the incomplete screening behavior at the long range. Setting the threshold parameter according to the static dielectric

constant of the system, we make the SCF iterations reach the convergence efficiently and independent of the system size. For metal-insulator hybrid systems, the idea of the "effective" conducting electrons is introduced to the module of the Thomas-Fermi wave vector in the original Kerker preconditioner. By estimating this module in the modified Kerker preconditioning scheme, we can achieve the SCF convergence within 30 iterations in the calculations of Au-MoS₂ slabs with a thickness of 160 Å, saving about 40% of the SCF iteration steps compared to the original Kerker scheme. When one does not have sufficient knowledge of the systems, we design a *a posteriori* indicator to monitor if the charge sloshing has been suppressed and to guide appropriate parameter setting. Based on the *a posteriori* indicator, we present two schemes of the self-adaptive configuration during the SCF iterations. The implementation of our approach requires only small modifications on the original Kerker scheme and the extra computational overhead is negligible.

This paper is organized as follows: In Section II, we will reformulate the Pulay mixing scheme to show the physical meaning of the preconditioner in solving the fixed point equation. In Section III, we will revisit the Thomas-Fermi and Resta screening models to extend the Kerker preconditioner to the non-metallic systems. In Section IV, the effectiveness and efficiency of our approach will be examined by numerical examples. A further discussion on this preconditioning technique and an introduction of the *a posteriori* indicator and self-adaptive configuration schemes will be given in Section V. Concluding remarks will be presented in the last section.

II. MATHEMATICAL FRAMEWORK

A. Simple mixing and preconditioning

Finding the solution of the Kohn-Sham equation where the output density $n^{\text{out}}(\mathbf{r})$ is equal to the input density $n^{\text{in}}(\mathbf{r})$ can be generalized to the following fixed point equation:

$$\mathbf{F}(\mathbf{x}) = \mathbf{x}, \quad (1)$$

where \mathbf{x} denotes a vector in many dimensions, e.g. the density is expanded in the dimensions of a set of plane waves. This becomes a minimization problem for the norm of the residual which is defined as like

$$\mathbf{R}(\mathbf{x}) \equiv \mathbf{F}(\mathbf{x}) - \mathbf{x}. \quad (2)$$

The simplest method for seeking the solution of Eq. (1) is the fixed point iteration:

$$\mathbf{x}_{m+1} = \mathbf{F}(\mathbf{x}_m). \quad (3)$$

In the region where \mathbf{F} is a linear function of \mathbf{x} and \mathbf{x}^* is the solution of Eq' (1), we have

$$\mathbf{x}_{m+1} - \mathbf{x}^* = \left(\frac{\delta \mathbf{F}}{\delta \mathbf{x}} \right)^m (\mathbf{x}_1 - \mathbf{x}^*).$$

Therefore, a necessary condition that guarantees the convergence of the fixed point iteration is

$$\sigma \left(\frac{\delta \mathbf{F}}{\delta \mathbf{x}} \right) < 1,$$

where $\sigma(A)$ is the spectral radius of the operator or matrix A . However, in the Kohn-Sham equations, the above condition is generally not satisfied [5].

However, the simple mixing can reach convergence as long as $\sigma \left(\frac{\delta \mathbf{F}}{\delta \mathbf{x}} \right)$ is bounded. The simple mixing scheme takes the form:

$$\mathbf{x}_{m+1} = \mathbf{x}_m + P \mathbf{R}(\mathbf{x}_m), \quad (4)$$

where P is the matrix whose size is equal to the number of basis functions. We define the Jacobian matrix:

$$J \equiv -\frac{\delta \mathbf{R}}{\delta \mathbf{x}} = I - \frac{\delta \mathbf{F}}{\delta \mathbf{x}}, \quad (5)$$

and denote its value at \mathbf{x}^* by J_* . When \mathbf{x}_m are sufficiently close to \mathbf{x}^* , the residual propagation of simple mixing Eq. (4) is given by:

$$\mathbf{R}(\mathbf{x}_{m+1}) \approx (I - J_* P) \mathbf{R}(\mathbf{x}_m). \quad (6)$$

In some literature [3, 5, 17], P is αI with α being a scalar parameter. Then it follows from Eq. (6) that the simple mixing will lead to convergence if:

$$\sigma(I - \alpha J_*) < 1. \quad (7)$$

If $\lambda(J_*)$ is an eigenvalue of J_* , then the inequality Eq. (7) indicates that:

$$\|1 - \alpha \lambda(J_*)\| < 1. \quad (8)$$

Note that $\lambda(J_*) > 0$ is referred to as the stability condition of the material in [21]. And it holds in most cases according to the analysis given in [5]. Consequently, Eq. (8) implies that:

$$0 < \alpha < \frac{2}{\lambda(J_*)}. \quad (9)$$

When $\lambda(J_*)$ is bounded, it is always possible to find a parameter α to ensure the convergence of the simple mixing scheme. Nevertheless, $\lambda(J_*)$ can become very large in practice, especially in the case of large scale metallic systems, which makes the convergence of the simple mixing extremely slow. Therefore it is desirable to construct effective preconditioning matrix P in Eq. (4) to speed up the convergence.

Here we will show that in the context of the charge mixing, the Jacobian matrix J is just the charge dielectric response function, which describes the charge response to an external charge perturbation. Replacing the \mathbf{x}_m in Eq. (4) with charge density \mathbf{n}_m yields

$$\mathbf{n}_{m+1} = \mathbf{n}_m + P \cdot \mathbf{R}(\mathbf{n}_m). \quad (10)$$

For $\mathbf{R}(\mathbf{n}_m)$, we could expand it near \mathbf{n} to the linear order

$$\mathbf{R}(\mathbf{n}) = \mathbf{R}(\mathbf{n}_m) - J \cdot (\mathbf{n} - \mathbf{n}_m). \quad (11)$$

Where J in the above equation is just the Jacobian matrix defined earlier in Eq. (5). We always want to achieve as much self-consistency as possible in the next step, such that $\mathbf{R}(\mathbf{n}_{m+1}) \approx 0$. Plugging this into Eq. (11), we have

$$\mathbf{n}_{m+1} = \mathbf{n}_m + J^{-1} \cdot \mathbf{R}(\mathbf{n}_m). \quad (12)$$

Comparing Eq. (12) with Eq. (10), we see that $P = J^{-1}$. The problem then becomes building a good approximation of the Jacobian matrix J . To show that J has the physical meaning of charge dielectric function, we follow Vanderbilt and Louie's procedure in Ref. [14]

$$\mathbf{V}_{m+1} \approx \mathbf{V}_m + U \cdot (\mathbf{n}_{m+1} - \mathbf{n}_m), \quad (13)$$

where the matrix U describe the change in the potential due to a change in the charge density. As a result, the output charge density is given by

$$\mathbf{n}_{m+1}^{\text{out}} \approx \mathbf{n}_m^{\text{out}} + \chi \cdot (\mathbf{V}_{m+1} - \mathbf{V}_m), \quad (14)$$

where χ is just the electric susceptibility matrix, describing the change in the output charge density due to a change in the potential. Combining Eqs. (10), (11), (13) and (14) yields

$$J = I - \chi \cdot U. \quad (15)$$

J is often called as the dielectric matrix. According to Vanderbilt and Louie [14], J^{-1} is the *charge* dielectric response function which describes the fluctuation in the total charge due to a perturbation from external charge. Adopting the potential mixing, we can also obtain a dielectric response function $(I - U \cdot \chi)^{-1}$ which describes the potential response to an external potential perturbation. Note that the order of the matrix product matters and generally the *charge* dielectric response function and *potential* dielectric response function are different but closely related.

B. Pulay mixing scheme

Instead of using vector \mathbf{x}_m only from last step in Eq. (4), we minimize the norm of the residual $\|\mathbf{R}(\mathbf{x})\|$ using the best possible combination of the \mathbf{x}_m from all previous steps. This is the idea behind the technique called Direct Inversion in the Iterative Subspace (DIIS). The technique is originally developed by Pulay to accelerate the Hartree-Fock calculation [10]. Hence it is often referred to as Pulay mixing in the condensed matter physics community.

An alternative way to derive Pulay method is taking it as the special case of the Broyden's method [22]. In the Broyden's second method, a sequence of low-rank modifications are made to modify initial guess of the inverse Jacobian matrix Eq. (5) near the solution of Eq. (1). The recursive formula [6, 23] can be derived from the following constrained optimization problem:

$$\begin{cases} \min_H \frac{1}{2} \|H - H_{m-1}\|_F^2 \\ \text{s.t. } HY_{m-1} = -S_{m-1}, \end{cases} \quad (16)$$

where H_{m-1} is the approximation to the inverse Jacobian in the $(m-1)$ th Broyden update, S_{m-1} and Y_{m-1} are respectively defined as:

$$\begin{aligned} S_{m-1} &= (\delta\mathbf{x}_{m-1}, \dots, \delta\mathbf{x}_{m-l+1}), \\ Y_{m-1} &= (\delta\mathbf{R}_{m-1}, \dots, \delta\mathbf{R}_{m-l+1}). \end{aligned} \quad (17)$$

It will be later proved in the appendix that the solution to Eq. (16) is:

$$H_m = H_{m-1} - (S_m + H_{m-1}Y_m) (Y_m^T Y_m)^{-1} Y_m^T. \quad (18)$$

We arrive at Pulay mixing scheme by fixing the H_{m-1} in Eq. (18) to the initial guess H_1 of the inverse Jacobian:

$$H_m = H_1 - (S_{m-1} + H_1 Y_{m-1}) (Y_{m-1}^T Y_{m-1})^{-1} Y_{m-1}^T. \quad (19)$$

Then one can follow the quasi Newton approach to generate the next vector:

$$\mathbf{x}_{m+1} = \mathbf{x}_m + H_m \mathbf{R}(\mathbf{x}_m) \quad (20)$$

$$= \mathbf{x}_m + H_1 \mathbf{R}(\mathbf{x}_m) - (S_{m-1} + H_1 Y_{m-1}) (Y_{m-1}^T Y_{m-1})^{-1} Y_{m-1}^T \mathbf{R}(\mathbf{x}_m). \quad (21)$$

We comment that the construction of H_1 in Eq. (21) is crucial for accelerating the convergence and is equivalent to the preconditioner for the simple mixing in Eq. (4). It is implied by Eq. (7) that preconditioning would be effective if H_1 is a good guess of the inverse dielectric matrix near the solution of Eq. (1). In this paper, we concentrate on the Kerker based preconditioning models and appropriate parameterization schemes to capture the long-range dielectric behavior, which turns out to be crucial in the SCF convergence.

III. PRECONDITIONING MODEL

A. Thomas-Fermi screening model

The Thomas-Fermi screening model is the foundation for the Kerker preconditioner. We first present the derivation of the Thomas-Fermi screening model, i.e. the dielectric response function of the homogeneous electron gas. In what follows, some key features of this screening model will be discussed.

Assume an external defect charge (or some small perturbation in the charge density) being introduced into a homogeneous electron gas. The external potential then solely arises from the external charge and satisfies Poisson's equation

$$-\nabla^2 V_{ext} = 4\pi n_{ext}(\mathbf{r}). \quad (22)$$

The external charge induces a cloud of screening electrons, resulting in redistribution of the total potential and charge density. Similarly, we have

$$-\nabla^2 V_{tot} = 4\pi n_{tot}(\mathbf{r}). \quad (23)$$

The difference between the total charge density and external charge density gives the induced charge density n_{ind} . One could assume that V_{tot} and V_{ext} are linearly related through the relation [24]

$$V_{ext}(\mathbf{r}) = \int d\mathbf{r}' \varepsilon(\mathbf{r}, \mathbf{r}') V_{tot}(\mathbf{r}'). \quad (24)$$

In the homogeneous electron gas, the dielectric matrix ε would only depends on the distance between the \mathbf{r} and \mathbf{r}' . Thus Eq. (24) becomes

$$V_{ext}(\mathbf{r}) = \int d\mathbf{r}' \varepsilon(\mathbf{r} - \mathbf{r}') V_{tot}(\mathbf{r}'). \quad (25)$$

It holds for their Fourier components:

$$V_{ext}(\mathbf{q}) = \varepsilon(\mathbf{q}) V_{tot}(\mathbf{q}). \quad (26)$$

If the perturbation is weak and slow-varying in real space, the induced charge density n_{ind} and the total potential V_{tot} are linearly linked by

$$n_{ind}(\mathbf{q}) = \chi(\mathbf{q}) V_{tot}(\mathbf{q}). \quad (27)$$

This relation shares the same idea with Eq. (14). The Fourier transforms of the Poisson Eqs. (22) and (23) are

$$\mathbf{q}^2 V_{ext}(\mathbf{q}) = 4\pi n_{ext}(\mathbf{q}), \quad (28)$$

$$\mathbf{q}^2 V_{tot}(\mathbf{q}) = 4\pi n_{tot}(\mathbf{q}). \quad (29)$$

Combining Eqs. (26), (27), (28) and (29), we have

$$\varepsilon(\mathbf{q}) = 1 - 4\pi \frac{\chi(\mathbf{q})}{\mathbf{q}^2}. \quad (30)$$

The dielectric matrix ε (or J in the context of previous section) can be diagonalized due to the homogeneity of the system and can be seen as a function of \mathbf{q} . Now we calculate the quantity $\chi(\mathbf{q})$. The induced charge density is the difference between systems with and without the external potential

$$n_{ind}(\mathbf{r}) = -e[N(\mu + eV(\mathbf{r})) - N(\mu)], \quad (31)$$

where the electron number density N as a function of chemical potential μ is given by the Fermi-Dirac distribution and dispersion relation of the free electron gas

$$N(\mu) = \int \frac{d\mathbf{k}}{4\pi^3} \frac{1}{\exp[\beta(\frac{\hbar^2 \mathbf{k}^2}{2m_e} - \mu)] + 1}. \quad (32)$$

Based on the assumption that the external potential is weak and slow-varying in space, we could expand Eq. (31) near the electron chemical potential μ (or the Fermi energy ε_F) to the first order as

$$n_{ind}(\mathbf{r}) = -e^2 \frac{\delta N}{\delta \mu} V(\mathbf{r}), \quad (33)$$

where the quantity $\frac{\delta N}{\delta \mu}$ is proportional to the number of states in the vicinity of the electronic chemical potential or Fermi level. Comparing Eqs. (33) and (27), we have

$$\chi(\mathbf{q}) = -e^2 \frac{\delta N}{\delta \mu}. \quad (34)$$

Thus, Eq. (30) now becomes

$$\varepsilon(\mathbf{q}) = 1 + \frac{k_{TF}^2}{\mathbf{q}^2}. \quad (35)$$

This is the dielectric function of the Thomas-Fermi screening model [44] where the Thomas-Fermi vector k_{TF} is defined through

$$k_{TF}^2 = 4\pi e^2 \frac{\delta N}{\delta \mu}. \quad (36)$$

Now we can derive Kerker preconditioner [4, 12, 17] by inverting the dielectric matrix

$$H_1^{TF}(\mathbf{q}) = \frac{\mathbf{q}^2}{\mathbf{q}^2 + k_{TF}^2}. \quad (37)$$

There are some remarks on the Thomas-Fermi screening model with its implication to Kerker preconditioner and SCF calculations:

- (i) It can be indicated by Eq. (35) that the dielectric function diverges quadratically at small \mathbf{q} , which is the mathematical root of the charge sloshing. If a metallic system contains small \mathbf{q} 's, the change in the input charge density will be magnified by the asymptotic divergence at long wavelength. This, in turn, results in large and long-range changes in the output charge density, known as the "charge sloshing". Such convergence issue is more prominent in the long-z metallic slab systems in which one dimension of the cell is much larger than the rest two. Therefore we use the slab systems for numerical tests.
- (ii) It is reasonable to ignore the contribution of the exchange-correlation potential during the derivation. In the long wavelength limit, this type of local potential is much smaller in magnitude compared to the Coulomb potential, which causes the $1/\mathbf{q}^2$ divergence at small \mathbf{q} . In this sense, the Thomas-Fermi screening as well as the Kerker preconditioning model correctly describe the dielectric behavior of metallic systems at long wavelength, which makes the Kerker preconditioner appropriate for the typical metallic systems.
- (iii) Even though the dielectric function in Eq. (35) is mounted on the homogeneous electron gas, it still manifests an important feature of the electron screening in the metallic systems. As mentioned above, $\frac{\delta N}{\delta \mu}$ has the physical meaning of the number of the states in the vicinity of (below and above) the Fermi level. Those electrons can actively involve in screening since

they can adjust themselves to higher unoccupied states to accommodate the change in the potential. On the other hand, deeper electrons are limited by the high excitation energy or Pauli exclusion principle. This observation is somehow independent of the band structures of the system.

(iv) Following the above point, we further estimate the parameter k_{TF} under the assumption of homogeneous electron gas. Since $\frac{\delta N}{\delta \mu}$ can be approximated by the number of states at the Fermi level, we can write k_{TF} as

$$k_{TF}^2 \approx 4\pi e^2 N(\varepsilon_F) = \frac{4(3\pi^2 n_0)^{1/3}}{a_B \pi}, \quad (38)$$

and

$$a_B = \hbar^2/(me^2) \approx 0.53 \text{ \AA}, \quad (39)$$

where a_B is the Bohr radius and n_0 is the total free electron density in the system. Plugging in numbers, we have the following relation:

$$k_{TF} \approx 2\left(\frac{n_0}{a_B^3}\right)^{1/6}. \quad (40)$$

In a typical metal, $n_0 \approx 10^{23} \text{ cm}^{-3}$. Therefore, $k_{TF} \approx 1 \text{ \AA}^{-1}$. This is also the default value for Kerker preconditioner in many simulation packages. As shown later, Eq. (40) could help us with parameterizing the k_{TF} and facilitate the convergence of the metal-insulator hybrid systems.

B. Resta screening model

The Thomas-Fermi screening model is more appropriate in describing the screening effect in the metallic system. Resta revised the boundary condition of the previous Poisson equation Eq. (23) and derived the screening model for semiconductors and insulators [25]. Rather than the complete screening in the metallic system, the potential is only partially screened beyond some screening length in the insulators. This is characterized by the static dielectric constant $\varepsilon(0)$

$$V(\mathbf{r}) = -\frac{Z}{\varepsilon(0)r}, \quad r \geq R_s, \quad (41)$$

where R_s is the screening length which is generally on the order of the lattice constants. According to Resta, the relation between the screening length and the static dielectric constant

is given by

$$\varepsilon(0) = \frac{\sinh(q_0 R_s)}{q_0 R_s}, \quad (42)$$

where q_0 is a constant related to the valence electron Fermi momentum k_F as follows

$$q_0 = (4k_F/\pi)^{1/2}. \quad (43)$$

k_F is related to the average valence electron density n_0 by

$$k_F = (3\pi n_0)^{1/3}. \quad (44)$$

Under the atomic unit, q_0 is in the unit of inverse distance. The dielectric function can be written as follow

$$\varepsilon(\mathbf{q}) = \frac{q_0^2 + \mathbf{q}^2}{\frac{q_0^2 \sin(|\mathbf{q}| R_s)}{\varepsilon(0) |\mathbf{q}| R_s} + \mathbf{q}^2}. \quad (45)$$

The three material parameters q_0 , R_s and $\varepsilon(0)$ in the above equation are related by Eq. (42) thus only two are needed for the input. The static dielectric constant $\varepsilon(0)$ and Fermi momentum related quantity q_0 can be extracted from the experimental data. In Resta's original paper, he offered the input parameters for Diamond, Silicon and Germanium. He further showed that the Resta's dielectric functions for these materials are in close agreement with others derived from Penn-model results of Srinivasan [26, 27] and RPA calculations of Walter and Cohen [28]. However, the dielectric function he proposed is much simpler in the expression compared with others. Later on, Shajan and Mahadevan [29] used Resta's model to calculate the dielectric function of many binary semiconductors, such as GaAs, InP, ZnS, etc. Their results are found to be in excellent agreement with those calculated by the empirical pseudopotential method [30].

Here, we proposed the Resta's preconditioner by inverting Eq. (45)

$$H_1^{Res}(\mathbf{q}) = \frac{\frac{q_0^2 \sin(|\mathbf{q}| R_s)}{\varepsilon(0) |\mathbf{q}| R_s} + \mathbf{q}^2}{q_0^2 + \mathbf{q}^2}. \quad (46)$$

It is instructive to compare this preconditioner with Kerker preconditioner. The two preconditioners are plotted as the function of \mathbf{q} in Fig. 1. For Kerker preconditioner, the k_{TF} is chosen to be 1, in the unit of \AA^{-1} . For the Resta preconditioner, the static dielectric constant is chosen to be 6.5. For many semiconductors and insulators, this value falls into the range of $5 \sim 15$. The q_0 is chosen to be 1\AA^{-1} and the screening length is 4\AA , accordingly. These values are about the typical inputs for all binary semiconductors studied in [29]. From

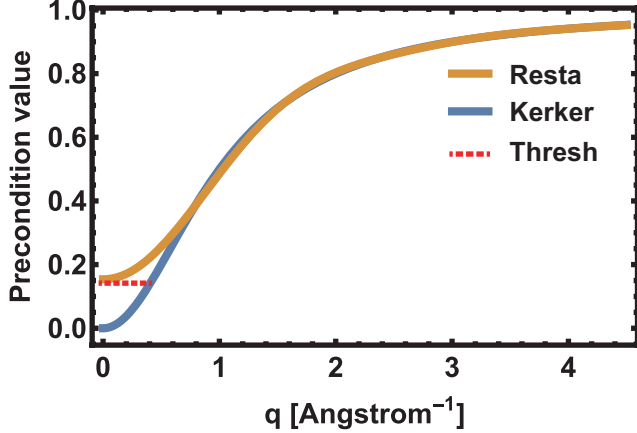


FIG. 1: (color online) The preconditioning models as a function of reciprocal vector \mathbf{q} . A threshold parameter can be added to the Kerker preconditioner to simulate the small \mathbf{q} behavior of the insulating systems.

Fig. 1, we would like to point out the following points:

- (i) The essential difference between the Kerker preconditioner and Resta preconditioner lies at the long wavelength limit. Kerker preconditioner, as we have discussed previously, goes to zero quadratically while the Resta preconditioner goes to $1/\varepsilon(0)$. This represents the incomplete screening in the insulating systems due to a lack of conducting electrons. If a nominal insulating system contains the defect states which are not completely filled, Resta preconditioner does not offer too much help in speeding up the convergence.
- (ii) A threshold can be added to the Kerker preconditioner to mimic the behavior of the Resta preconditioner at the small \mathbf{q} 's, as shown by the dashed line in the Fig. 1. Now the modified Kerker preconditioner takes the form:

$$H_1^{TF'}(\mathbf{q}) = \max(a_0, \frac{\mathbf{q}^2}{\mathbf{q}^2 + k_{TF}^2}). \quad (47)$$

This action restores the behavior of the screening effect in the insulating systems. A more practical variant includes the linear mixing parameter α together with the preconditioner:

$$H_1^{TF''}(\mathbf{q}) = \max(a_0, \alpha \frac{\mathbf{q}^2}{\mathbf{q}^2 + k_{TF}^2}). \quad (48)$$

Accordingly, the optimal a_0 should be around $\alpha/\varepsilon(0)$. This modification extends the applicability of Kerker preconditioner to insulating systems.

TABLE I: The number of convergence steps in the Au slab systems using original Kerker preconditioner.

Number of Au layers	Total slab thickness [Å]	Number of steps
14	50	27
36	110	32
54	150	31

IV. NUMERICAL EXAMPLES

We have performed the convergence tests on various systems using the in-house code CESSP [31, 32] under the infrastructure of JASMIN [33]. The exchange and correlation energy is described by the generalized gradient approximation proposed by Perdew, Burke, and Ernzerhof [34]. Electron-ion interactions are treated with projector augmented wave potentials [35]. The first 5 steps take the block variant [36] of the Davison algorithm with no charge mixing. The following steps take the RMM-DIIS method [3] with charge mixing. The mixing parameter α is set to 0.4 in all calculations with different preconditioners. The convergence criterion for self-consistent field loop is 1×10^{-6} eV, which is sufficient for most slab calculations. Each of our slab model includes at least 20 Å of vacuum layer to exclude the spurious interaction under the periodic boundary condition. Along the x and y directions the cells are kept as primitive cell in all calculations.

A. Au slab: the metallic system

The first system is the $\{111\}$ Au slab. We have constructed three Au slab systems with 14, 33 and 54 layer of Au $\{111\}$ planes, corresponding to a cell parameter of 50, 110 and 150 Å along the direction normal to Au $\{111\}$ surface, respectively. A $12 \times 12 \times 1$ k-point grid is used to sample the Brillouin zone. The cutoff energy is 350 eV. We take the modified Kerker preconditioner with $a_0 = 0$, referred as "original" Kerker preconditioner, to speed up the SCF convergence for such long- z metallic slabs. The k_{TF} has been set to 1 in the unit of Å⁻¹. The number of iterations to reach the convergence is listed in Table I.

If we try Pulay mixing scheme with the preconditioning matrix αI , the SCF convergence cannot be reached within 120 steps for any slab. Thus the Kerker preconditioner does

significantly improve the convergence for the long- z Au systems. In addition, the number of steps from Kerker preconditioner is weakly dependent on the size of the system, which also imply that the charge sloshing has been well suppressed. As stated in the previous section, the Thomas-Fermi model and the Kerker preconditioner catch the asymptotic behavior of the dielectric function at long wavelength limit, even though the free electron gas model is not a good approximation for Au as well as most metallic systems.

B. MoS_2 : the layered insulating system

Secondly, we have studied the convergence of the layered insulating system: MoS_2 . Two slab systems with 10 and 20 layers of MoS_2 , corresponding to a cell parameter of 80 Å and 160 Å, have been constructed. The MoS_2 layers have been stacked in the same fashion as those in the bulk MoS_2 . A $6 \times 6 \times 1$ k-point grid has been used to sample the Brillouin zone. The cutoff energy is 450 eV. Both Kerker and Resta preconditioners have been tested on the MoS_2 slab systems.

For the Resta preconditioner, we need the static dielectric constant and screening length as input parameters. We find the reported value of the average static elastic constant of MoS_2 varying in literature [37–40]. It is also found that this value depends on the number of MoS_2 layers. However, they all fall into the range of $5 \sim 15$. Thus we have used three static dielectric constants 5, 10 and 15, in the Resta preconditioner. The screening length R_s has been set to 3.5 which is close to the lattice constants. The q_0 in the Resta model is then calculated by Eq. (42).

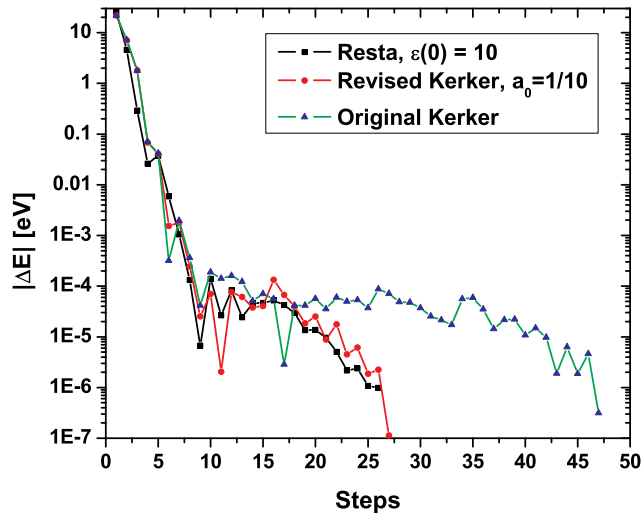
We adopt both the original and modified Kerker preconditioners. In both preconditioners, the Thomas-Fermi vector k_{TF} has been set to 1 \AA^{-1} . In the modified Kerker preconditioner, we have chosen the threshold parameters a_0 according to the dielectric constants in the Resta model. The threshold parameters a_0 are 0.4/5, 0.4/10 and 0.4/15 accordingly.

We further plot the convergence of energies between three preconditioning model in Fig. 2. For the modified Kerker model and the Resta model, we choose the results from those with dielectric constant of 10. The first 5 steps use the blocked Davison scheme thus we plot the energy versus steps from the 6th step.

It can be seen from Table II and Fig. 2 that the Resta model and the modified Kerker model make the energy converge faster than the original Kerker scheme, since the MoS_2

TABLE II: The number of convergence steps in the MoS₂ slab systems.

Precondition model	10 layer MoS ₂	20 layer MoS ₂
Original Kerker	38	52
Resta($\varepsilon(0) = 5$)	25	26
Resta($\varepsilon(0) = 10$)	30	31
Resta($\varepsilon(0) = 15$)	32	32
Modified Kerker ($a_0 = 0.4/5$)	27	27
Modified Kerker ($a_0 = 0.4/10$)	28	32
Modified Kerker ($a_0 = 0.4/15$)	28	32


 FIG. 2: (color online) The convergence of energies in 20 layer MoS₂ correponding to different preconditioning models.

slab systems are insulating in nature. These two models give a correct behavior of the incomplete screening effect for insulators at small \mathbf{q} . In addition, using 5, 10 or 15 for the static dielectric constant gives similar results, indicating that the convergence speed is less sensitive to corresponding parameters.

C. Si slab: the insulating system containing defect states

Even though Resta preconditioner seems to be more appropriate for insulating systems, we show that this is not the case for the "nominal" insulating systems containing defect

states crossing the Fermi level. To illustrate this, we construct a 96 layer Si slab with the $\{111\}$ orientation and a cell parameter of 175 Å along z direction. Both the top and bottom Si surfaces have one dangling bond due to the creation of the surface. A $6 \times 6 \times 1$ k-point grid has been used to sample the Brillouin zone. The cutoff energy is 320 eV. The dielectric constant of bulk Si is about 12. The screening length R_s is set to 4.2 Å and the q_0 is set to 1.1 \AA^{-1} according to Resta's work [25]. We compare the convergence speed between the three preconditioning models and the results are shown in Table III.

TABLE III: The number of convergence steps in the original and H-passivated Si slab system.

Preconditioning model	Original Si slab	H-passivated Si slab
Original Kerker	40	46
Modified Kerker ($a_0 = 0.4/12$)	52	29
Resta	47	30

The original Kerker preconditioner offers the fastest convergence compared with the rest two, which goes against with the conclusion from the previous section. After careful inspection, we find that it is the surface states of the Si slab that deviate the system from a "perfect" insulating system. The density of states (DOS) of the Si slab and the partial charge density of the surface states have been plotted in Fig. 3(a). We can see that the creation of the surface introduces defect states right at the Fermi level. The presence of these states drives the system away from a "perfect" insulating system, since the states right at the Fermi level is finite. This essential difference makes the preconditioning models designed for insulators much less effective. In our previous case, since the MoS₂ is naturally layered, we will not introduce surface states when creating slabs from the bulk.

To further prove our idea, we passivate the Si surface states through covering the surface with H atoms. Now the system contains 96 layer of Si with 2 extra layer of H covering the top and bottom Si surfaces. The convergence speed versus different preconditioning models is also shown in the Table III. Now the trend is consistent with that of MoS₂: the modified Kerker (29 steps) and Resta models (30 steps) works better than the original Kerker model (46 steps). The extra H layers have passivated the dangling bonds on the Si surfaces thus removed the surface states. This is clearly shown by the DOS of the H passivated Si slab in Fig. 3(b).

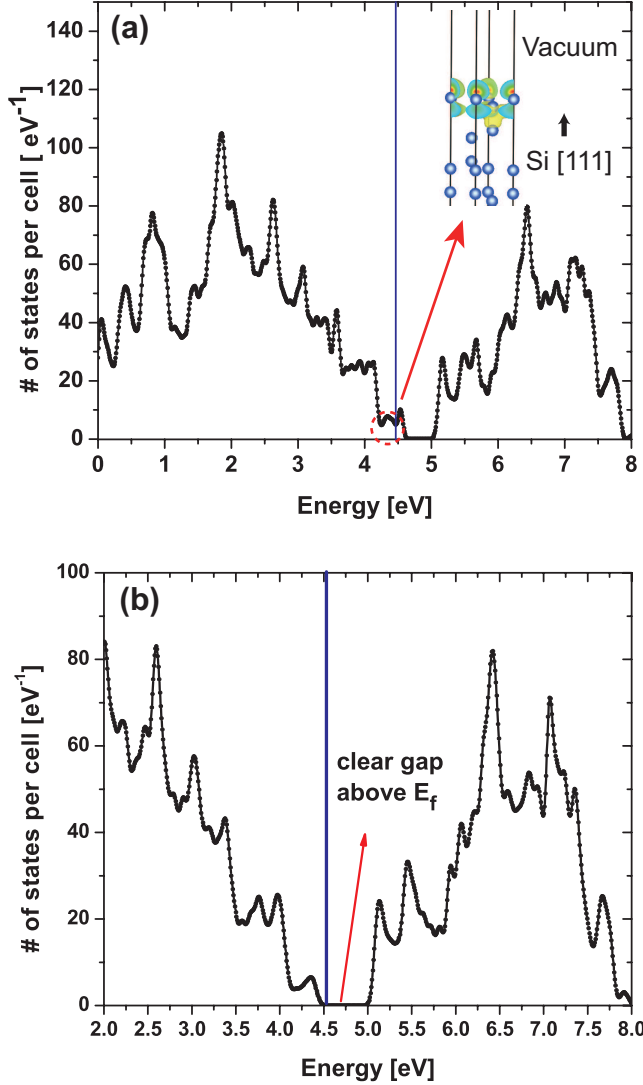


FIG. 3: (color online) (a) The DOS of the 96-atom Si slab. The vertical blue line indicates the Fermi level. The states right below the Fermi level are the surface states, as shown by the partial charge density plot. The bottom surface is identical to the top surface thus only one is shown. (b) The DOS of the Si slab with H passivation (96 layer of Si with 2 H passivation layer on the top and bottom Si surfaces). The added H layers remove the surface states: a clear band gap now occurs right above Fermi level.

Given this, the modified Kerker preconditioner and Resta preconditioner are better suited for the "prefect" insulating systems. However, introducing conducting states crossing the Fermi level from defects would render these preconditioning models much less effective.

D. Au-MoS₂: the metal-insulator hybrid system

Finally we come to Au-MoS₂ contact systems that combine multiple layers of Au in {111} orientation and multiple layers of MoS₂. The Au layers and MoS₂ layers are in close contact, separated by a distance of the covalent bond length. Such structural models have been studied using DFT calculations to understand the surface, interface and contact properties of Au-MoS₂ epitaxial systems [41–43]. The Au-MoS₂ contact configuration is similar to the {111} orientation configuration in Ref. [42]. To investigate the performance of the preconditioning, we have constructed slab systems that are much thicker.

Au-MoS₂ slabs with different fraction of Au and MoS₂ have been created. These slab systems share the same cell parameters and nearly same slab thickness and total number of atoms. The total length of the cell is 160 Å with ~ 25 Å vacuum layer and ~ 135 Å Au-MoS₂ slab. The total number of atoms is about 65 with slight variation in different slabs. We use the following notation to label slabs with different fraction of Au and MoS₂: X Au + Y MoS₂ means we have X layer of Au and Y layer of MoS₂ in the slab. The total number of atoms is $X + 3Y$ since each MoS₂ contains 3 layer of atom. A $6 \times 6 \times 1$ k-point grid is used to sample the Brillouin zone. The cutoff energy is 450 eV. Here we only consider the Kerker preconditioner and its modified version. Resta model is no longer appropriate to describe Au-MoS₂ hybrid systems. As shown later, it is possible to achieve fast convergence of such highly inhomogeneous systems under the Kerker preconditioning model, even though the model is originally based on the homogeneous electron gas.

There are two parameters in the modified Kerker preconditioner to adjust: a_0 and k_{TF} , according to Eqs. (37) and (47). Since these two parameters are describing the effectiveness of the screening from different perspective, we will be only adjusting one parameter while keep the other fixed.

Firstly we keep $k_{TF} = 1$ Å⁻¹ and estimate the lower and upper bounds of a_0 . We consider two extremes where the system is solely Au and MoS₂, respectively. In the former case, a_0 can be chosen any value below $\alpha \frac{q_{min}^2}{q_{min}^2 + k_{TF}^2}$, where q_{min} is the reciprocal vector along z direction. Thus the lower bound is about 6×10^{-4} with $q_{min} = 2\pi/L$ and $L = 160$ Å. In the latter case, a_0 can be set to be 0.04 if the static dielectric constant is chosen as 10. Nevertheless, it is difficult to determine the optimized value of a_0 for systems with varying Au fraction. Reducing a_0 to the original Kerker preconditioner leads to convergence in all

cases, though generally it is not the most efficient one. Consequently the lower bound can be regarded as a safe choice since .

Secondly we keep $a_0 = 0$ and adjust k_{TF} . According to Eq. (40), k_{TF} is related to the number of electrons participating in the screening. Starting from the system of solely Au, increasing the proportion of MoS₂ part means a reduction in the number of "free" electrons for screening, and resulting in a decreasing value of k_{TF} . For solely Au slab, the value of k_{TF} is 1 Å⁻¹. Replacing a fraction, say $1 - f$, of the Au slab with MoS₂, reduces the number of free electrons n to fn since the MoS₂ makes no contributions to the screening electrons. Therefore, the k_{TF} for the hybrid system can be calculated as $k_{TF} \times f^{1/6}$, according to Eq. (40). For example, in the 27 Au + 12 MoS₂ system, there are total 63 atoms in the system. Thus the Au fraction is 27/63 and the corresponding k_{TF} is given by $(\frac{27}{63})^{(1/6)} \sim 0.87$. The results are listed in Table IV together with the results from the original Kerker scheme.

TABLE IV: The convergence speed in Au-MoS₂ hybrid systems versus k_{TF} and a_0 .

Au-MoS ₂ systems	Original Kerker	Adjusting k_{TF} ^a
43 Au + 6 MoS ₂	34	33 (0.94)
39 Au + 8 MoS ₂	41	39 (0.92)
27 Au + 12 MoS ₂	49	29 (0.87)
16 Au + 16 MoS ₂	43	41 (0.8)
11 Au + 18 MoS ₂	32	31 (0.74)
7 Au + 19 MoS ₂	48	31 (0.70)
5 Au + 20 MoS ₂	47	34 (0.65)
3 Au + 21 MoS ₂	37	45 (0.60)
1 Au + 22 MoS ₂	37	22 (0.50)

^aThe estimated values of k_{TF} are shown in the parenthesis.

Adjusting k_{TF} in such way offers at least comparable and, most likely, faster convergence compared with original Kerker scheme. In the low Au fraction slabs (1, 3, 5, and 7 layers), our scheme saves about 22% of overall SCF steps with respect to the original Kerker scheme. With increasing fraction of Au, these two schemes exhibit similar performance as the slabs now become closer to bulk metals. In our opinion, adjusting k_{TF} would be potentially

preferred in some kind of high-throughput calculations.

Moreover, in the 3 Au + 21 MoS₂ system, we previously ignore the contribution of interface states to the "effective" free electrons. Therefore, slightly increasing k_{TF} could optimize our preconditioner. When changing k_{TF} from 0.6 to 0.65, the convergence steps become 32, faster than the 37 steps from original Kerker scheme. Similarly, in the 16 Au + 16 MoS₂ system, changing k_{TF} from 0.8 to 0.85 reduces the convergence steps from 41 to 31. We further note that adopting this parameterization scheme requires *a priori* knowledge of the system. The parameterization scheme for situations without sufficient *a priori* knowledge will be discussed later.

V. FURTHER DISCUSSIONS

We would like to address few important points in this section:

1. The Thomas-Fermi screening model and modified Kerker preconditioner

The Thomas-Fermi screening model and the Kerker preconditioner is rooted in the homogeneous electron gas model. It can be shown by numerical examples that with some simple but physically meaningful modifications, the Kerker preconditioner can be applied to a wide range of materials. All test systems are no way near the free electron gas system, such as the insulating systems and the metal-insulator contact systems. Then what is the merit in the modified Kerker preconditioner? We believe that a good description of the long-range screening behavior is key to fast convergence. While in the modified Kerker scheme, it is possible to capture the essence of long-range screening: the original Kerker scheme naturally suppress quadratic divergence as $\mathbf{q} \rightarrow 0$ in the metallic system; the incomplete screening effect in the insulating systems is represented by the threshold parameter a_0 ; in the metal-insulator contact system, the long-range screening effect is characterized by the parameter k_{TF} which represents the number of effective electrons participating in the screening. The numerical examples indeed prove the effectiveness of the modified Kerker preconditioner: converging a large-scale slab system (with more than 60 layer and more than 150 Å long in cell parameter) to relatively high accuracy in about 30 SCF steps is significant for practical applications. Also, in many Au-MoS₂ cases, the modified Kerker scheme (when k_{TF} is reasonably set) speed up 40% compared to the original Kerker scheme.

2. *A posteriori* indicator and self-adaptive configuration

In practice, it may be difficult to appropriately parameterize the preconditioner when lacking *a priori* knowledge. However, we can still monitor if the charge sloshing occurs during the SCF iterations by an *a posteriori* indicator. Theoretically, the charge sloshing is indicated by the spectrum of the matrix JP or its inverse $(JP)^{-1}$ from Eq. (6). Practically, we compute the eigenvalues of $P^{-1}H_m$ instead of $(JP)^{-1}$. The preconditioning matrix P is a symmetric positive definite with the Kerker scheme or our modified version. The matrix H_m updated by Eq. (19) satisfies the constraint condition in Eq. (16):

$$H_m Y_{m-1} = -S_{m-1}. \quad (49)$$

Assuming the vectors \mathbf{x}_{m-i} all sufficiently close to the solution of Eq. (1), we have

$$J^{-1}Y_{m-1} \approx -S_{m-1}. \quad (50)$$

Comparing Eq. (49) with Eq. (50), we find that H_m is almost the best approximation of the inverse Jacobian J^{-1} in the subspace spanned by Y_{m-1} . Consequently the eigenvalues of $P^{-1}H_m$ are calculated in this subspace by solving the following generalized eigenvalue problem:

$$Y_{m-1}^T H_m Y_{m-1} \mathbf{u}_i = \lambda_i Y_{m-1}^T P Y_{m-1} \mathbf{u}_i. \quad (51)$$

In implementation, we shift Eq. (51) as like

$$Y_{m-1}^T (H_m - P) Y_{m-1} \mathbf{u}_i = (\lambda_i - 1) Y_{m-1}^T P Y_{m-1} \mathbf{u}_i. \quad (52)$$

Note that it takes little computational overhead on solving Eq. (52) since $(H_m - P)Y_{m-1} = -(S_{m-1} + H_1 Y_{m-1})$ has been calculated in Pulay's update and the dimension of Eq. (52) is generally less than 50 in our code.

As far as we know, Kresse and Furthmüller [3] propose similar formula as Eqs.(51) and (52) to investigate the spectrum range for insulators and open-shell transition metals of different sizes. Instead of examining the range of spectrum, we extract the minimal module of the eigenvalues from Eq. (51). This value is the *a posteriori* indicator to show whether the preconditioner have suppressed charge sloshing or not. If charge sloshing occurs, the *a posteriori* indicator would be on or below the order of 0.01 due to the divergence of the dielectric function. With the *a posteriori* indicator, the SCF convergence can be achieved through self-adaptive schemes.

We demonstrate the *a posteriori* indicator in calculations of the 5 Au + 20 MoS₂ system. The energy convergence and the minimal eigenvalue of the Jacobian matrix during the SCF calculation under different a_0 are plotted in Fig. 4. Before doing the calculation, one would

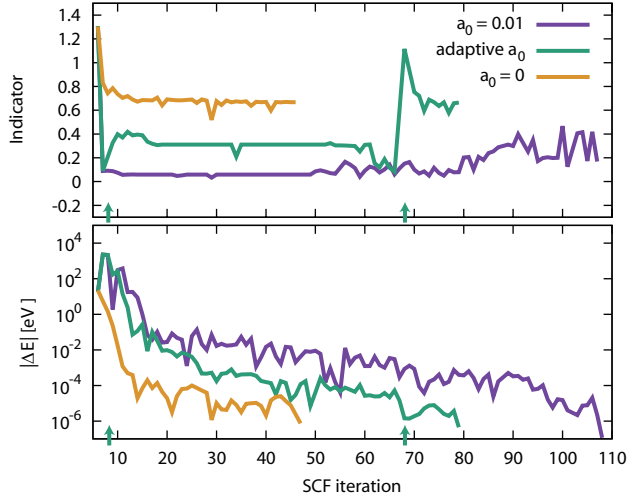


FIG. 4: (color online) The *a posteriori* indicator (a) and the energy convergence (b) versus SCF iteration step under $a_0 = 0.01$, and two self-adaptive schemes are shown. The arrows on the axis indicate that we launch self-adaptive configuration at the 8th step and 67th step.

guess the 5 Au + 20 MoS₂ system is similar to the solely MoS₂ system since the major part is MoS₂. Then, we begin with the threshold parameter $a_0 = 0.01$. It is illustrated in Fig. 4 that the SCF convergence with $a_0 = 0.01$ is slow while the *a posteriori* indicator is lying below 0.1 at most of the first 80 SCF steps, which implies an incomplete suppression of the charge sloshing.

If the *a posteriori* indicator is less than 0.1, two the self-adaptive schemes come into play. One is to stop the current one and restart with original Kerker preconditioner (corresponding to "adaptive 1" in Fig. 4). After the self-adaptive configuration at the 8th step, the *a posteriori* indicator is kept around 0.7 and the convergence is remarkably accelerated. The other way is to clear the subspace Y_{m-1} and continue SCF iteration with original Kerker preconditioner (corresponding to "adaptive 2" in Fig. 4). Two self-adaptive configurations occur at the 8th step and 67th step to keep the *a posteriori* indicator at relative high values. The SCF convergence is finally reached around 80 steps, still saves about 30 steps compared with the $a_0 = 0.01$ run. The former scheme seems more efficient than the latter for now. Further studies on the self-adaptive configuration in the SCF calculations will be presented

elsewhere.

3. Integrated preconditioning scheme

Here we present the complete strategy of the modified Kerker preconditioning in Table V. We add some remarks on this integrated strategy:

TABLE V: The general parameterization strategy for large dimension systems.

No.	System	Long-range screening properties	Preconditioner
1	Metal	$1/q^2$	Original Kerker
2	Insulator	$\epsilon(0)$	Modified Kerker or Resta
3	Metal + insulator	Effective "free" e^-	$k_{TF} = f^{1/6}$
4	Unknown	Unknown	$a_0 \sim 0.04$ & <i>a posteriori</i> indicator

- (i) The threshold parameter a_0 for insulators can be set to 0.04 in default. The static dielectric constant for most insulators fall into the range between $5 \sim 15$, and the SCF convergence is not that sensitive to static dielectric constant. Therefore, we expect that the default setting can also help to achieve fast convergence in many insulating systems.
- (ii) We discuss the metal-insulator hybrid where the metal region and insulator region are spatially separated and well defined, such as the metal-insulator contact systems shown above. A fine mixing of them on the scale of atomic distance does not fall into this category. Such situation should be treated as a system lack of *a priori* knowledge unless further information can be founded.
- (iii) Strategy 4 basically presumes the system is insulator. Then the SCF iteration is monitored by the *a posteriori* indicator. If the charge sloshing occurs, the preconditioning scheme will be self-adaptively reconfigured. For now we suggest using "adaptive 1", which discards the current calculation and restart with original Kerker preconditioner. Moreover, developing effective self-adaptive scheme is of great significance for future studies.

VI. CONCLUSIONS

We have proposed the modified Kerker scheme to improve the SCF convergence for metallic, insulating and metal-insulator hybrid systems. The modifications contain three key points: the original Kerker preconditioner is suited for typical metallic systems; the thresh-

old parameter a_0 characterizes the screening behavior of insulators at long wavelength limit thus helps to accommodate the insulating systems; the k_{TF} represents the effective number of conducting electrons and its approximation can be used to improve the SCF convergence for metal-insulator hybrid systems; the *a posteriori* indicator guides the inexperienced users away from staggering in the charge sloshing. The modifications cost negligible extra computation overhead and exhibit the flexibility of working in either *a priori* or self-adaptive way, which would be favored by the high-throughput first-principles calculations.

ACKNOWLEDGEMENTS

This work was partially supported by Science Challenge Project under Grant JCKY2016212A502, the National Key Research and Development Program of China under Grant 2016YFB0201204, the National Science Foundation of China under Grants 91730302 and 11501039, the China Postdoctoral Science Foundation under Grant 2017M610820.

APPENDIX

Now we prove that Eq. (18) is the solution to the constraint optimization problem Eq. (16). It is prerequisite to prove the following lemma.

Lemma 1. *Let $X \in \mathbb{C}^{m \times n}$, $A \in \mathbb{C}^{n \times p}$, $B \in \mathbb{C}^{m \times p}$, and assume that A has full column rank. Denote the Moore-Penrose pseudoinverse of A by A^\dagger with $A = (A^H A)^{-1} A^H$. If $XA = B$ is satisfiable, and the matrix $Z \equiv BA^\dagger$, then it holds that*

$$\|Z\|_F \leq \|X\|_F \quad (53)$$

Proof. Let $Q \equiv AA^\dagger$. Then it follows that $Q^H = Q$ and $ZQ = Z$. Thus we have

$$\begin{aligned}
(X - Z, Z)_F &\equiv \text{tr} [(X - Z)Z^H] \\
&= \text{tr} [(X - Z)(ZQ)^H] \\
&= \text{tr} [(X - Z)Q^HZ^H] \\
&= \text{tr} [(X - Z)QZ^H] \\
&= \text{tr} [(XAA^\dagger - ZQ)Z^H] \\
&= \text{tr} [(BA^\dagger - Z)Z^H] \\
&= 0
\end{aligned} \tag{54}$$

Note that Eq. (55) is an inner product corresponding to the Frobenius norm $\|\cdot\|_F$. Hence

$$\begin{aligned}
\|X\|_F^2 &= \|X - Z\|_F^2 + 2(X - Z, Z)_F + \|Z\|_F^2 \\
&= \|X - Z\|_F^2 + \|Z\|_F^2 \\
&\geq \|Z\|_F^2
\end{aligned}$$

with equality if and only if $X = Z$. □

Let $H' \equiv H - H_{m-1}$. Thus the optimization problem (16) can be replaced by its equivalent one

$$\begin{cases} \min_{H'} \|H'\|_F^2 \\ \text{s.t. } H'Y_{m-1} = -(S_{m-1} + H_{m-1}Y_{m-1}), \end{cases} \tag{55}$$

It follows from Lemma 1 that the solution to the problem Eq. (55) is

$$H' = -(S_{m-1} + H_{m-1}Y_{m-1}) (Y_{m-1}^T Y_{m-1})^{-1} Y_{m-1}^T. \tag{56}$$

Therefore the solution to the problem (16) is

$$H = H_{m-1} - (S_{m-1} + H_{m-1}Y_{m-1}) (Y_{m-1}^T Y_{m-1})^{-1} Y_{m-1}^T. \tag{57}$$

[1] P. Hohenberg and W. Kohn, Phys. Rev. **136**, B864 (1964), URL <https://link.aps.org/doi/10.1103/PhysRev.136.B864>.

[2] W. Kohn and L. J. Sham, Phys. Rev. **140**, A1133 (1965), URL <https://link.aps.org/doi/10.1103/PhysRev.140.A1133>.

[3] G. Kresse and J. Furthmüller, Phys. Rev. B **54**, 11169 (1996), URL <https://link.aps.org/doi/10.1103/PhysRevB.54.11169>.

[4] G. Kresse and J. Furthmüller, Computational Materials Science **6**, 15 (1996), ISSN 0927-0256, URL <http://www.sciencedirect.com/science/article/pii/0927025696000080>.

[5] J. F. Annett, Computational Materials Science **4**, 23 (1995), ISSN 0927-0256, URL <http://www.sciencedirect.com/science/article/pii/0927025694000133>.

[6] L. D. Marks and D. R. Luke, Phys. Rev. B **78**, 075114 (2008), URL <https://link.aps.org/doi/10.1103/PhysRevB.78.075114>.

[7] P. J. Hasnip, K. Refson, M. I. J. Probert, J. R. Yates, S. J. Clark, and C. J. Pickard, Philosophical Transactions of the Royal Society of London A: Mathematical, Physical and Engineering Sciences **372** (2014), ISSN 1364-503X, <http://rsta.royalsocietypublishing.org/content/372/2011/20130270.full.pdf>, URL <http://rsta.royalsocietypublishing.org/content/372/2011/20130270>.

[8] J. K. Norskov, F. Abild-Pedersen, F. Studt, and T. Bligaard, Proceedings of the National Academy of Sciences **108**, 937 (2011), <http://www.pnas.org/content/108/3/937.full.pdf>, URL <http://www.pnas.org/content/108/3/937.abstract>.

[9] C. G. Van de Walle and R. M. Martin, Phys. Rev. B **34**, 5621 (1986), URL <https://link.aps.org/doi/10.1103/PhysRevB.34.5621>.

[10] P. Pulay, Chemical Physics Letters **73**, 393 (1980), ISSN 0009-2614, URL <http://www.sciencedirect.com/science/article/pii/0009261480803964>.

[11] C. G. Broyden, Math. Comp. **19**, 577 (1965).

[12] G. P. Kerker, Phys. Rev. B **23**, 3082 (1981), URL <https://link.aps.org/doi/10.1103/PhysRevB.23.3082>.

[13] D. Raczkowski, A. Canning, and L. W. Wang, Phys. Rev. B **64**, 121101 (2001), URL <https://link.aps.org/doi/10.1103/PhysRevB.64.121101>.

[14] D. Vanderbilt and S. G. Louie, Phys. Rev. B **30**, 6118 (1984), URL <https://link.aps.org/doi/10.1103/PhysRevB.30.6118>.

[15] X. Gonze, B. Amadon, P.-M. Anglade, J.-M. Beuken, F. Bottin, P. Boulanger, F. Bruneval, D. Caliste, R. Caracas, M. Ct, et al., Computer Physics Communications

180, 2582 (2009), ISSN 0010-4655, 40 YEARS OF CPC: A celebratory issue focused on quality software for high performance, grid and novel computing architectures, URL <http://www.sciencedirect.com/science/article/pii/S0010465509002276>.

[16] Y. Shiihara, O. Kuwazuru, and N. Yoshikawa, Modelling and Simulation in Materials Science and Engineering **16**, 035004 (2008), URL <http://stacks.iop.org/0965-0393/16/i=3/a=035004>.

[17] L. Lin and C. Yang, SIAM Journal on Scientific Computing **35**, S277 (2013), URL <http://dx.doi.org/10.1137/120880604>, URL <http://dx.doi.org/10.1137/120880604>.

[18] K.-M. Ho, J. Ihm, and J. D. Joannopoulos, Phys. Rev. B **25**, 4260 (1982), URL <https://link.aps.org/doi/10.1103/PhysRevB.25.4260>.

[19] A. Sawamura and M. Kohyama, Mater. Trans. **45**, 1422 (2004).

[20] P.-M. Anglade and X. Gonze, Phys. Rev. B **78**, 045126 (2008), URL <https://link.aps.org/doi/10.1103/PhysRevB.78.045126>.

[21] R. B. R and R. Ahlrichs, J. Chem. Phys. **104**, 9047 (1996).

[22] D. D. Johnson, Phys. Rev. B **38**, 12807 (1988).

[23] H. Fang and Y. Saad, Numer. Linear. Algebra Appl. **16**, 197 (2009).

[24] L. LANDAU and E. LIFSHITZ, *Electrodynamics of Continuous Media (Second Edition Revised and Enlarged)*, vol. 8 (Pergamon, 1984), second edition revised and enlarged ed.

[25] R. Resta, Phys. Rev. B **16**, 2717 (1977), URL <https://link.aps.org/doi/10.1103/PhysRevB.16.2717>.

[26] D. R. Penn, Phys. Rev. **128**, 2093 (1962), URL <https://link.aps.org/doi/10.1103/PhysRev.128.2093>.

[27] G. SRINIVASAN, Phys. Rev. **178**, 1244 (1969), URL <https://link.aps.org/doi/10.1103/PhysRev.178.1244>.

[28] J. P. Walter and M. L. Cohen, Phys. Rev. B **2**, 1821 (1970), URL <https://link.aps.org/doi/10.1103/PhysRevB.2.1821>.

[29] X. S. Shajan and C. Mahadevan, Crystal Research and Technology **27**, 253 (1992), ISSN 1521-4079, URL <http://dx.doi.org/10.1002/crat.2170270217>.

[30] P. K. W. Vinsome and D. Richardson, Journal of Physics C: Solid State Physics **4**, 2650 (1971), URL <http://stacks.iop.org/0022-3719/4/i=16/a=030>.

[31] J. Fang, X. Gao, H. Song, and H. Wang, The Journal of Chemical Physics **144**, 244103 (2016), URL <http://dx.doi.org/10.1063/1.4954234>, URL <http://dx.doi.org/10.1063/1.4954234>.

[32] X. Gao, Z. Mo, J. Fang, H. Song, and H. Wang, Computer Physics

Communications **211**, 54 (2017), ISSN 0010-4655, high Performance Computing for Advanced Modeling and Simulation of Materials, URL <http://www.sciencedirect.com/science/article/pii/S0010465516301837>.

[33] Z. Mo, A. Zhang, X. Cao, Q. Liu, X. Xu, H. An, W. Pei, and S. Zhu, Frontiers of Computer Science in China **4**, 480 (2010), ISSN 1673-7466, URL <http://dx.doi.org/10.1007/s11704-010-0120-5>.

[34] J. P. Perdew, K. Burke, and M. Ernzerhof, Phys. Rev. Lett. **77**, 3865 (1996), URL <http://link.aps.org/doi/10.1103/PhysRevLett.77.3865>.

[35] G. Kresse and D. Joubert, Phys. Rev. B **59**, 1758 (1999), URL <http://link.aps.org/doi/10.1103/PhysRevB.59.1758>.

[36] B. Liu, in *Numerical Algorithms in Chemistry: Algebraic Methods*, edited by E. Moler and I. Shavitt (Lawrence Berkley Lab. Univ. of California, 1978), p. 49.

[37] A. Molina-Sánchez and L. Wirtz, Phys. Rev. B **84**, 155413 (2011), URL <https://link.aps.org/doi/10.1103/PhysRevB.84.155413>.

[38] T. Cheiwchanchamnangij and W. R. L. Lambrecht, Phys. Rev. B **85**, 205302 (2012), URL <https://link.aps.org/doi/10.1103/PhysRevB.85.205302>.

[39] L. Liang and V. Meunier, Nanoscale **6**, 5394 (2014), URL <http://dx.doi.org/10.1039/C3NR06906K>.

[40] N. Saigal, V. Sugunakar, and S. Ghosh, Applied Physics Letters **108**, 132105 (2016), <http://dx.doi.org/10.1063/1.4945047>, URL <http://dx.doi.org/10.1063/1.4945047>.

[41] I. Popov, G. Seifert, and D. Tománek, Phys. Rev. Lett. **108**, 156802 (2012), URL <http://link.aps.org/doi/10.1103/PhysRevLett.108.156802>.

[42] Y. Zhou, D. Kiriyama, E. E. Haller, J. W. Ager, A. Javey, and D. C. Chrzan, Phys. Rev. B **93**, 054106 (2016), URL <https://link.aps.org/doi/10.1103/PhysRevB.93.054106>.

[43] J. Kang, W. Liu, D. Sarkar, D. Jena, and K. Banerjee, Phys. Rev. X **4**, 031005 (2014), URL <https://link.aps.org/doi/10.1103/PhysRevX.4.031005>.

[44] Strictly speaking, the ε derived here is respect to the potential. However, under the condition of homogeneous system, the potential dielectric response function and charge dielectric response function are same. This is because the χ in Eq. (15) becomes diagonalized thus the product of $\chi \cdot U$ equals to $U \cdot \chi$.